Hyperfine Interact (2016) 237:61
DOI 10.1007/s10751-016-1292-7

Role of iron in $Na_{1.5}Fe_{0.5}Ti_{1.5}(PO_4)_3$/C as electrode material for Na-ion batteries studied by operando Mössbauer spectroscopy

Siham Difi[1,2] · Ismael Saadoune[2,5] · Moulay Tahar Sougrati[1,3] · Rachid Hakkou[2] · Kristina Edstrom[4] · Pierre-Emmanuel Lippens[1,3]

Abstract The role of iron in $Na_{1.5}Fe_{0.5}Ti_{1.5}(PO_4)_3$/C electrode material for Na batteries has been studied by ^{57}Fe Mössbauer spectroscopy in operando mode. The potential profile obtained in the galvanostatic regime shows three plateaus at different voltages due to different reaction mechanisms. Two of them, at 2.2 and 0.3 V vs Na^+/Na^0, have been associated to redox processes involving iron and titanium in $Na_{1.5}Fe_{0.5}Ti_{1.5}(PO_4)_3$. The role of titanium was previously elucidated for $NaTi_2(PO_4)_3$ and the effect of the substitution of Fe for Ti was investigated with ^{57}Fe Mössbauer spectroscopy. We show that iron is an electrochemically active center at 2.2 V with the reversible Fe^{3+}/Fe^{2+} transformation and then remains at the oxidation state Fe^{2+} along the sodiation until the end of discharge at 0 V.

Keywords Electrode · NASICON · Phosphate · Na-ion batteries · Mössbauer spectroscopy · in situ

This article is part of the Topical Collection on *Proceedings of the International Conference on the Applications of the Mössbauer Effect (ICAME 2015), Hamburg, Germany, 13–18 September 2015*

✉ Pierre-Emmanuel Lippens
lippens@univ-montp2.fr

[1] Institut Charles Gerhardt, UMR 5253 CNRS, Université de Montpellier, Place Eugène Bataillon, cedex 5, 34095 Montpellier, France

[2] Laboratoire de Chimie des Matériaux et de l'Environnement, Université Cadi Ayyad, Avenue A. Khattabi, BP 549 Marrakech, Morocco

[3] Réseau sur le Stockage Electrochimique de l'Energie (RS2E), FR 3459 CNRS, Cedex, 80039 Amiens, France

[4] Department of Chemistry - Ångström laboratory, Uppsala University, Box 538, SE 751 21, Uppsala, Sweden

[5] Center for Advanced Materials, Université Mohammed VI Polytechnique, Lot 660-Hay Moulay Rachid, Ben Guerir, Morocco

Published online: 24 February 2016

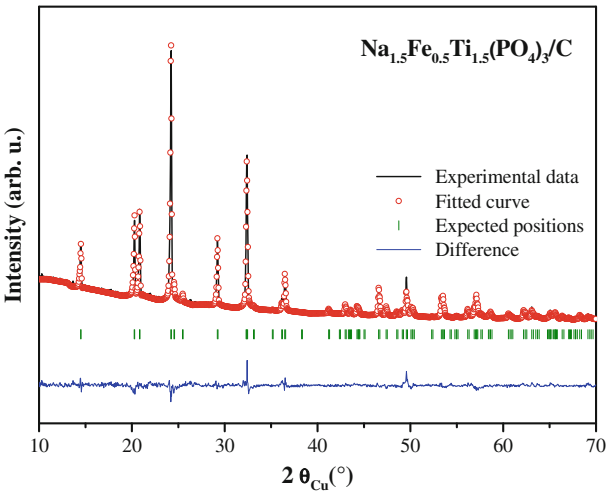

Fig. 1 XRD pattern of $Na_{1.5}Fe_{0.5}Ti_{1.5}(PO_4)_3$/C

1 Introduction

Li-ion batteries provide high energy density and are now widely used for electrical energy storage. However, the development of sustainable and renewable energy sources strongly increases the demand for lithium. Unfortunately, lithium resources are limited and unevenly distributed worldwide. In addition, the cost and the safety of lithium storage systems could be the major drawbacks for large-scale applications [1]. In that context, rechargeable Na-ion batteries can be considered a serious alternative in the future because of the low cost and natural abundance of sodium as well as the improved safety of the batteries with the use of aqueous electrolytes [2].

The need for new electrode materials with high specific capacity, low irreversible loss, high coulombic efficiency and long cycle life is crucial for the development of the Na-ion technology. NASICON (Na Super Ionic Conductors) type materials with the formula unit $Na_xM_y(PO_4)_3$, where M is a transition metal, have attracted a considerable attention because of their high ionic conductivity and the possibility of tuning the operation voltage by changing M [3]. The structure of $Na_xM_y(PO_4)_3$ can be described as a three-dimensional framework of corner sharing MO_6 octahedra and PO_4 tetrahedra with interconnected channels for the diffusion of Na^+ ions. $NaTi_2(PO_4)_3$ is an interesting example because of its promising electrochemical performances and its peculiar potential profile [4–6]. The potential curve exhibits a plateau at about 2.1 V vs Na^+/Na^0 fixed by the redox potential of Ti^{4+}/Ti^{3+} and a theoretical specific capacity of 133 mAh g^{-1}, and another plateau at about 0.4 V due to the Ti^{3+}/Ti^{2+} redox couple which has not been widely investigated. As a consequence, the composition $Na_3Ti_2(PO_4)_3$ can be used in a symmetrical electrochemical cell involving the reversible reactions $NaTi_2(PO_4)_3 \leftrightarrow Na_3Ti_2(PO_4)_3$ at the cathode and $Na_3Ti_2(PO_4)_3 \leftrightarrow Na_4Ti_2(PO_4)_3$ at the anode [6]. However, this material suffers from some limitations such as poor electronic conductivity and needs improvements for practical applications.

The present paper concerns the analysis of the electrochemical reaction mechanisms of $Na_{1.5}Fe_{0.5}Ti_{1.5}(PO_4)_3$/C composite as electrode material for Na-ion batteries in the

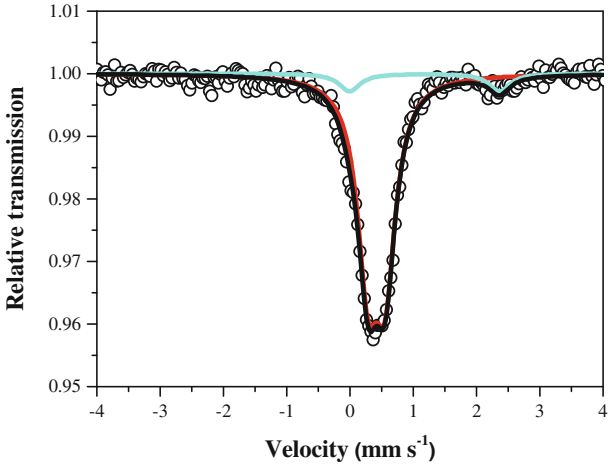

Fig. 2 ^{57}Fe Mössbauer spectrum of $Na_{1.5}Fe_{0.5}Ti_{1.5}(PO_4)_3$/C at room temperature: experimental data (open circles), total fitted curve (black line), Fe^{3+} (red line) and Fe^{2+} (cyan line) subspectra

potential range 0–3 V. The substitution of Fe for Ti and the carbon coating increase the ionic and electronic conductivity, respectively, and both improve the electrochemical performances as shown previously for the potential plateau at ∼2.2 V [7, 8]. The present work supplements these studies by considering the overall potential range. A particular attention is devoted to the effect of Fe for Ti substitution studied by ^{57}Fe Mössbauer spectroscopy in operando mode, which is a unique tool to analyze electrochemical reaction mechanisms in batteries at the atomic scale [9–13].

2 Experimental

$Na_{1.5}Fe_{0.5}Ti_{1.5}(PO_4)_3$ was prepared by solid-state reaction from stoichiometric amounts of Na_2CO_3, $(NH_4)_2HPO_4$, Fe_2O_3 and TiO_2 precursors heated at 400 °C under air for 12 h in an open alumina crucible and cooled to room temperature. The product was then hand-ground and heated at 600 °C for 12 h and, after cooling at room temperature, reground and calcined at 1000 °C for 12 h to obtain a pure powder of $Na_{1.5}Fe_{0.5}Ti_{1.5}(PO_4)_3$. The carbon coating was obtained by mixing this powder with 15 wt% of sucrose in acetone, drying the solution for the evaporation of acetone and heating the product at 500 °C for 6 h in flowing argon.

The X-ray diffraction (XRD) patterns were collected under Bragg-Brentano geometry at 2θ in the range 12–120° with PHILIPS X'Pert MPD equipped with the X'celerator detector using Ni filter and Cu-Kα radiation ($\lambda = 1.5418$ Å). The microstructure was analyzed with a scanning electron microscope (SEM) and the specific surface area of the powdered samples was evaluated with the Brunauer Emmett Teller (BET) method from nitrogen physisorption measurements at 77 K with a Micrometric ASAP 2020. The residual carbon content was determined from thermogravimetric analysis (TGA) with a heating rate of 10 °C min^{-1} using a thermal analyzer Labsys.

The ^{57}Fe Mossbauer spectra were recorded in transmission geometry and a constant acceleration mode at room temperature with ^{57}Co (Rh) γ source. The velocity scale was

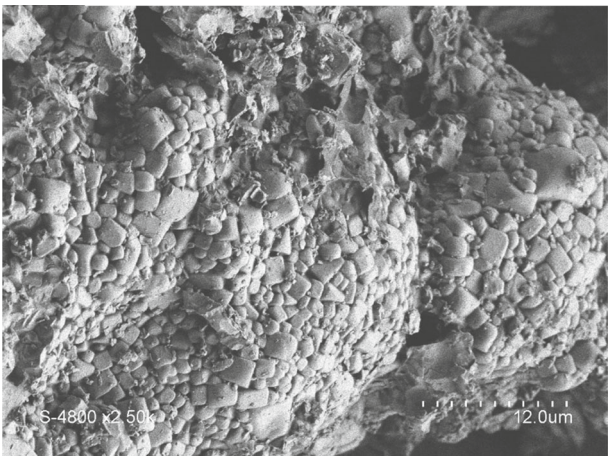

Fig. 3 SEM image of $Na_{1.5}Fe_{0.5}Ti_{1.5}(PO_4)_3$/C

calibrated using high-purity iron foil absorber as a standard at room temperature. The values of isomer shift (δ), quadrupole splitting (Δ), full line width at half-maximum (Γ) and relative area (RA) were determined by fitting Lorentzian lines to the experimental data with a nonlinear least-square method. The values of the isomer shift are given with respect to α-Fe.

The working electrodes were prepared by mixing 80 wt% active material and 20 wt% Super P carbon powder. A specific electrochemical cell was used for *in situ* ^{57}Fe Mössbauer spectroscopy [14] that was assembled inside the dry box under controlled argon atmosphere by using a sodium foil as the counter electrode, a borosilicate glass microfiber sheet (Whattman) as the separator and an organic electrolyte with 1M $NaClO_4$ dissolved in a solution of propylene carbonate (PC) and 5 vol% of fluoroethylene carbonate (FEC) as additive. The Mössbauer data were collected for one discharge-charge cycle in the range 1–3 V, followed by a full discharge until 0 V performed in the galvanostatic mode at C/25 (1 Na/f.u. in 25 h), during time steps of 4 h. Thus, each spectrum corresponds to the insertion (discharge) or extraction (charge) of 0.16 Na/f.u.

3 Results and discussion

The X-ray diffraction pattern of $Na_{1.5}Fe_{0.5}Ti_{1.5}(PO_4)_3$/C was indexed in the rhombohedral system with the space group $R\bar{3}c$ giving the lattice constants a = 8.53 Å, c = 21.77 Å (Fig. 1). The observed increase of a, compared to $NaTi_2(PO_4)_3$ (a = 8.48 Å), is in agreement with the substitution of Fe^{3+} (ionic radius: 0.645 Å) for Ti^{4+} (ionic radius: 0.605 Å). No additional XRD peaks that could be assigned to impurities have been observed. The ^{57}Fe Mössbauer spectrum of $Na_{1.5}Fe_{0.5}Ti_{1.5}(PO_4)_3$/C measured at room temperature shows a main band centered at ~0.5 mm s^{-1} and a small peak at ~2.3 mm s^{-1} (Fig. 2). The spectrum was fitted to two doublets. The isomer shift of the main doublet (91% relative area) δ = 0.42(1) mm s^{-1} and the quadrupole splitting Δ = 0.28(1) mm s^{-1} can be assigned to high spin Fe^{3+} ions in slightly distorted FeO_6 octahedra that substitute for Ti in $Na_{1.5}Fe_{0.5}Ti_{1.5}(PO_4)_3$. The Mössbauer parameters of the small doublet (9% relative area): δ = 1.18(1) mm s^{-1} and Δ = 2.37(1) mm s^{-1} are typical of high spin Fe^{2+} in intrinsic defects or external impurities arising from the sucrose pyrolysis. It is worth noting that the

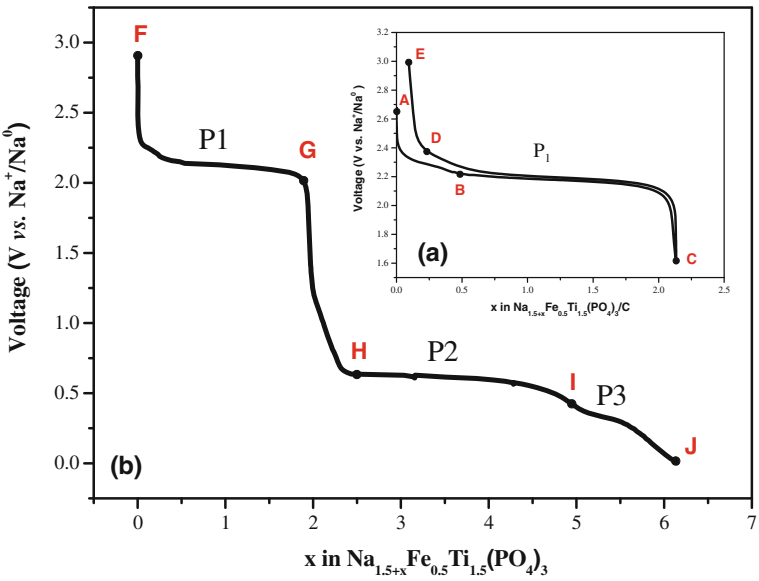

Fig. 4 Voltage profile of $Na_{1.5}Fe_{0.5}Ti_{1.5}(PO_4)_3$/C obtained in the galvanostatic regime at C/10 for the potential window 0 - 3 V including the first reversible first cycle (**a**) and the full discharge (**b**). The potential plateaus are labelled P1 (2.2 V), P2 (0.6 V) and P3 (0.3 V). The points indicate the stages of sodiation for the selected Mössbauer spectra of Fig. 6

Fe^{2+} contribution was not observed for $Na_{1.5}Fe_{0.5}Ti_{1.5}(PO_4)_3$ before pyrolysis. The SEM image shows that $Na_{1.5}Fe_{0.5}Ti_{1.5}(PO_4)_3$/C is formed by aggregates of submicrometer-sized particles (Fig. 3). The amount of carbon was estimated to 2 wt% and the graphitization rate was controlled by Raman spectroscopy that shows a D/G intensity ratio similar to that observed for other carbon coated electrode materials [8]. Finally, the measured BET specific area of $\sim$20 m^2g^{-1} is two orders of magnitude higher than that of $Na_{1.5}Fe_{0.5}Ti_{1.5}(PO_4)_3$ before pyrolysis. These results reveal the high porosity of the electrode material and the quality of the carbon coating that are expected to improve electrolyte impregnation and electronic percolation, respectively.

The potential profile of the first discharge obtained in the galvanostatic regime at C/10 shows three plateaus at $\sim$ 2.2 V (P1), $\sim$0.6 V (P2) and $\sim$0.3 V (P3), respectively (Fig. 4). A similar profile was obtained for $NaTi_2(PO_4)_3$, and in this case the three plateaus were assigned to the reduction of Ti^{4+} to Ti^{3+} (P1), the formation of the surface electrolyte interphase (SEI) at the carbon black surface (P2) and the reduction of Ti^{3+} to Ti^{2+} (P3) ending with the electrolyte decomposition [6]. In order to analyze the effect of the substitution of Fe for Ti upon the reaction mechanisms, the ^{57}Fe Mössbauer spectroscopy was used in operando mode for the first electrochemical cycle at $\sim$2.2 V and for the full discharge. The spectra are all formed by a doublet for which the asymmetry only changes along P1 (Fig. 5). The Fe^{2+} impurities are electrochemically inactive and give a constant contribution to the spectra, which clearly occurs at the beginning of discharge and at the end of charge for P1. Thus, all the spectra were fitted to three doublets corresponding to Fe^{3+}, Fe^{2+} arising from the reduction of Fe^{3+} and Fe^{2+} impurities, respectively (Fig. 6).

The process taking place at P1 concerns $\sim$2 Na/f.u., which corresponds to a specific capacity of 125 mAh g^{-1} close to the theoretical capacity. Some selected Mössbauer

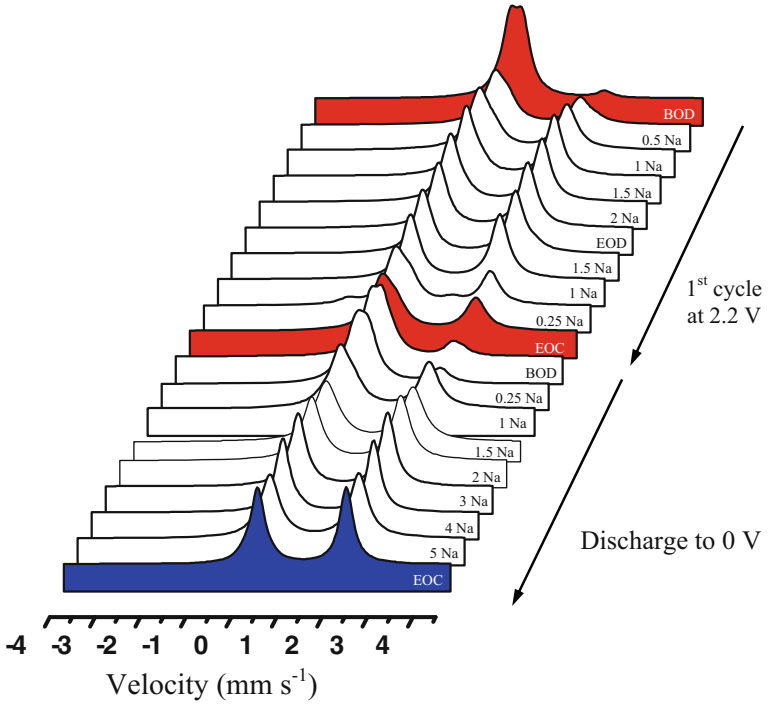

Fig. 5 Operando ^{57}Fe Mössbauer fitted spectra of $Na_{1.5}Fe_{0.5}Ti_{1.5}(PO_4)_3$/C recorded along the first reversible cycle and the full discharge with the galvanostatic current of C/25. BOD, EOC and EOD mean beginning of discharge, end of charge and end of discharge, respectively

spectra collected along the first reversible discharge-charge cycle show reversible changes of the Fe oxidation state from Fe^{3+} to Fe^{2+} for the discharge (reduction) and Fe^{2+} to Fe^{3+} for the charge (oxidation) (Fig. 6a). The Mössbauer parameters of Fe^{2+} arising from the electrochemical reduction of Fe^{3+} do not show any notable changes along this cycle and the average values are: $\delta = 1.25$ mm s^{-1} and $\Delta = 2.05$ mm s^{-1}. They are typical of high spin Fe^{2+} in FeO_6 octahedral environment as expected from the transfer of one electron to Fe^{3+} associated with Na^+ insertion. This reduction occurs at the beginning of the discharge ($x < 0.5$ Na/f.u.) while the Fe^{2+} oxidation occurs at the end of charge in the same range of inserted Na amount. This indirectly suggests that Ti^{4+}/Ti^{3+} redox couple is active for $0.5 < x < 2$ Na/f.u. The successive reductions of Fe^{3+} and Ti^{4+} along the discharge and the successive oxidations of Ti^{3+} and Fe^{2+} along the charge can be related to the close values of the redox potentials, which is however slightly higher for Fe^{3+}/Fe^{2+} (2.33 V *vs* Na^+/Na^0) than Ti^{4+}/Ti^{3+} (2.18 V *vs* Na^+/Na^0). Thus, the substitution of Fe for Ti does not significantly change the potential profile of P1 compared to $NaTi_2(PO_4)_3$ although the reaction mechanism combines monophasic and two-phase reactions typical of Fe and Ti based NASICON, respectively [6, 15].

The Mössbauer spectra obtained along the plateau P2 do not show any changes (Fig. 6b) and reflect the electrochemical inactivity of Fe^{2+}. This result indicates that side reactions occur at this potential, which is consistent with the electrolyte decomposition and SEI formation as previously observed at this potential for $NaTi_2(PO_4)_3$ [6]. The decomposition of

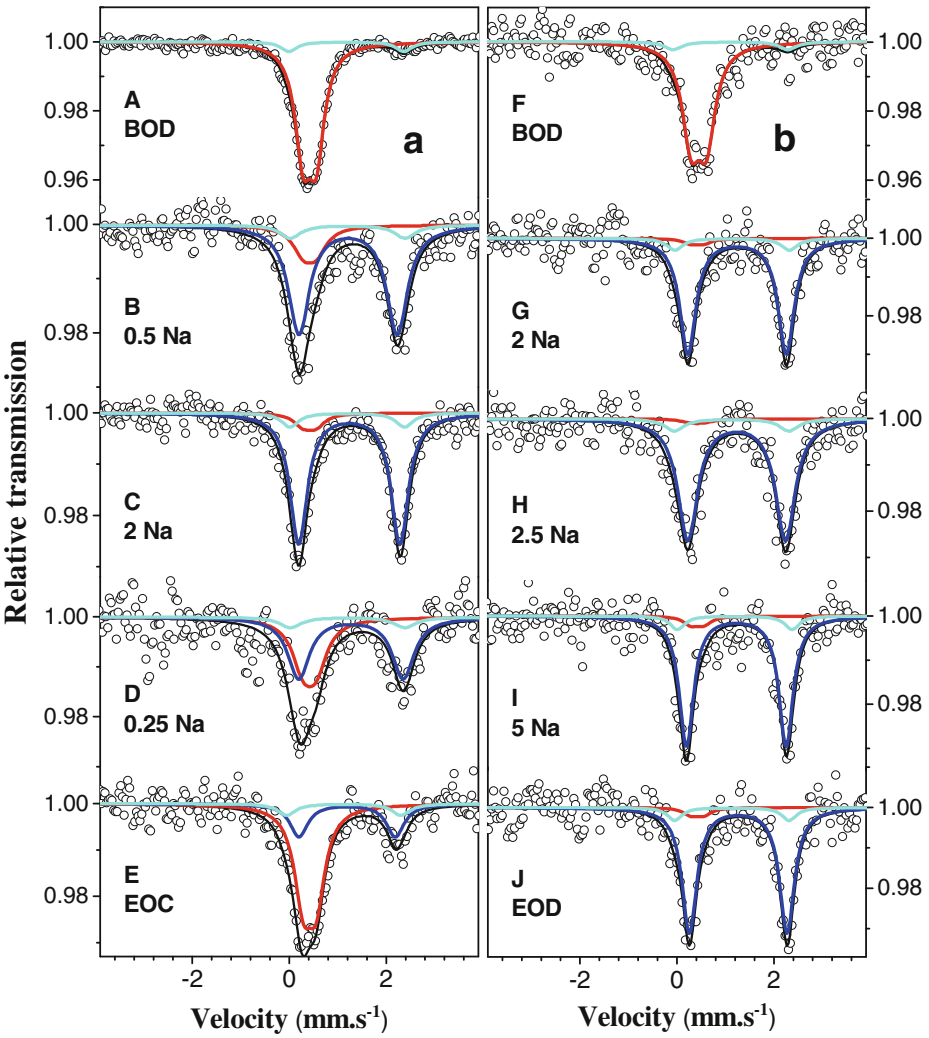

Fig. 6 Selected operando ^{57}Fe Mössbauer spectra of $Na_{1.5}Fe_{0.5}Ti_{1.5}(PO_4)_3$/C for different stages of sodiation along the first reversible cycle at P1 (**a**) and along the full discharge (**b**). The experimental data were fitted to three doublets corresponding to Fe^{3+} (*red line*), Fe^{2+} arising from the electrochemical reduction of Fe^{3+} (*blue line*) and Fe^{2+} impurities (*cyan line*). BOD, EOC and EOD mean beginning of discharge, end of charge and end of discharge, respectively

$NaClO_4$/PC/FEC based electrolyte used with tin electrode has been recently investigated by X-ray photoelectron spectroscopy (XPS) [16]. The reported results show that the SEI formation can be related to the decomposition of both PC and FEC although in the latter case FEC limits the PC decomposition and improves the electrochemical performances. Thus, this mechanism is irreversible and leads to a capacity loss that should be taken into account if $Na_{1.5}Fe_{0.5}Ti_{1.5}(PO_4)_3$/C is cycled at low potential. Possible solutions to reduce this capacity loss are the use of over-sodiated $Na_{1.5+x}Fe_{0.5}Ti_{1.5}(PO_4)_3$/C as starting material or modifications of the electrolyte or the electrode formulation. In $NaTi_2(PO_4)_3$, the

plateau P3 concerns Ti^{3+}/Ti^{2+} reduction. In the present case, the Mössbauer spectra of $Na_{1.5}Fe_{0.5}Ti_{1.5}(PO_4)_3$/C still not show any changes in Fe^{2+} oxidation state (Fig. 6b). This suggests that only Ti^{3+} is electrochemically active at this potential. Unlike P1, the reduction of titanium is not associated to that of iron for P3. Finally, the potential drops until 0 V with the insertion of less than 1 Na/f.u. The Mössbauer spectrum obtained at the end of discharge is still typical of Fe^{2+}, which means that neither Ti^{2+} nor Fe^{2+} were reduced by Na insertion at potential close to 0 V. This result differs from the Mössbauer spectra obtained for iron oxide based electrodes that show the formation of Fe^0 due to conversion reaction [17] and confirms that the full discharge is based on the progressive occupation of interstitial sites as observed for $NaTi_2(PO_4)_3$ [6]. At such low potential some side reactions due to the irreversible decomposition of the electrolyte could explain the observed smooth voltage decrease and participate to the SEI growth.

4 Conclusion

The reaction mechanism of $Na_{1.5}Fe_{0.5}Ti_{1.5}(PO_4)_3$/C composite considered as possible positive or negative electrode for Na-ion batteries has been investigated by ^{57}Fe Mössbauer spectroscopy in operando mode. The potential curve obtained for the full discharge shows three different plateaus that have been assigned to the Fe^{3+}/Fe^{2+} followed by Ti^{4+}/Ti^{3+} reversible transformations at 2.2 V, the SEI formation due to irreversible electrolyte decomposition at 0.6 V and the Ti^{3+}/Ti^{2+} reversible transformation at 0.3 V, respectively. Iron is only electrochemically active along the first plateau where it improves the electrochemical performances. To use $Na_{1.5}Fe_{0.5}Ti_{1.5}(PO_4)_3$/C at lower potential, parasitic side reactions should be reduced since they use a large amount of Na but further experiments are needed to understand these mechanisms.

Acknowledgments Financial supports by Campus France (PHC Toubkal 008/SM/13), the Centre National de la Recherche Scientifique (CNRS, France), the Centre National de la Recherche Scientifique et Technique (CNRST, Maroc), the Institut de Recherche en Energie Solaire et en Energies Nouvelles (IRESEN, Maroc), the Swedish Research Council (contract 2012-3392) and StandUp for Energy (Sweden) are gratefully acknowledged. This work was granted access to the HPC resources of CINES under the allocation c2014099131 made by GENCI (CINES, France) for providing computational resources.

References

1. Pan, H., Hu, Y.S., Chen, L.: Energy Environ. Sci. **6**, 2338 (2013)
2. Yabuuchi, N., Kubota, K., Dahbi, M., Komaba, S.: Chem. Rev. **114**, 11636 (2014)
3. Goodenough, J.B., Hong, H.Y.P., Kafalas, J.A.: Mater. Res. Bull. **11**, 203 (1976)
4. Delmas, C., Cherkaoui, F., Nadiri, A., Hagenmuller, P.A.: Mater. Res. Bull. **22**, 631 (1987)
5. Pang, G., Yuan, C., Nie, P., Ding, B., Zhu, J., Zhang, X.: Nanoscale **6**, 6328 (2014)
6. Senguttuvan, P., Rousse, G., Arroyo y de Dompablo, M.E., Vezin, H., Tarascon, J.M., Palacin, M.R.: J. Am. Chem. Soc. **135**, 3897 (2013)
7. Aragon, M.J., Vidal-Abarca, C., Lavela, P., Tirado, J.L.: J. Power Sources **252**, 208 (2014)
8. Difi, S., Saadoune, I., Sougrati, M.T., Hakkou, R., Edström, K., Lippens, P.E.: J. Phys. Chem. C **119**, 25220–25234 (2015)
9. Ionica-Bousquet, C.M., Lippens, P.E., Aldon, L., Olivier-Fourcade, J., Jumas, J.C.: Chem. Mater. **18**, 6442 (2006)
10. Aboulaich, A., Robert, F., Lippens, P.E., Aldon, L., Olivier-Fourcade, J., Willmann, P., Jumas, J.C.: Hyperfine Interac. **167**, 733 (2006)

11. Lippens, P.E., El Khalifi, M., Chamas, M., Perea, A., Sougrati, M.T., Ionica-Bousquet, C., Aldon, L., Olivier-Fourcade, J., Jumas, J.C.: Hyperfine Interac. **206**, 35 (2012)
12. Chamas, M., Sougrati, M.T., Reibel, Lippens, P.E.: Chem. Mater. **25**, 2410 (2013)
13. Philippe, B., Mahmoud, A., Ledeuil, J.B., Sougrati, M.T., Edström, K., Dedryvère, R., Gonbeau, D., Lippens, P.E.: Electrochim. Acta **123**, 72 (2014)
14. Leriche, J.B., Hamelet, S., Shu, J., Morcrette, M., Masquelier, C., Ouvrard, G., Zerrouki, M., Soudan, P., Belin, S., Elkaïm, E., Baudelet, F.: J. Electrochem. Soc. **157**, A606 (2010)
15. Patoux, S., Rousse, G., Leriche, J.B., Masquelier, C.: Chem. Mater. **15**, 2084 (2003)
16. Vogt, L.M., El Kazzi, M., Jämstorp Berg, E., Pérez Villar, S., Novák, P., Villevieille, C.: Chem. Mater. **27**, 1210 (2015)
17. López, M.C., Lavela, P., Ortiz, G.F., Tirado, J.L.: Electrochem. Commun. **27**, 152 (2013)